

Measuring Accretion in Young Substellar Objects: Approaching the Planetary Mass Regime ¹

James Muzerolle², Kevin L. Luhman³, César Briceño⁴, Lee Hartmann³, Nuria Calvet³

ABSTRACT

We present observations of H α emission line profiles taken at Magellan Observatory for a sample of 39 young low-mass stars and brown dwarfs in the Taurus and Chamaeleon I star forming regions. We have identified 11 new substellar accretors, more than tripling the number of known brown dwarfs with measurable accretion activity. These include the lowest-mass objects yet seen with accretion, with masses down to $\sim 0.015 M_{\odot}$. Using models of H α emission produced in magnetospheric accretion flows, the most widely applicable primary calibrator now available, we determine the first estimates of mass accretion rates for objects at such extremely low masses. For the six objects with masses $\lesssim 0.03 M_{\odot}$, we find accretion rates of $\sim 5 \times 10^{-12} M_{\odot} \text{ yr}^{-1}$, among the smallest yet measured. These new results continue the trend of decreasing mass accretion rate with decreasing (sub)stellar mass that we have noted previously for samples of more massive objects; the overall correlation is $\dot{M} \propto M^{2.1}$, and now extends over a mass range of over two orders of magnitude. Finally, the absence of a discontinuity in the distribution of accretion rates with mass tends to suggest that stars and brown dwarfs share similar formation histories.

Subject headings: accretion disks, brown dwarfs, stars: emission-line, pre-main sequence, circumstellar matter,

¹Based on observations performed at Las Campanas Observatory. This publication makes use of data products from the Two Micron All Sky Survey.

²Steward Observatory, 933 N. Cherry Ave., The University of Arizona, Tucson, AZ 85721

³Harvard-Smithsonian Center for Astrophysics, 60 Garden St., Cambridge, MA 02138

⁴Centro de Investigaciones de Astronomía (CIDA),
Apartado Postal 264, Mérida 5101-A, Venezuela

1. Introduction

The subject of the formation of substellar objects has garnered significant attention in the past few years. It remains unclear whether brown dwarfs form from the collapse of very low mass cloud cores, such as produced by turbulent fragmentation (Padoan & Nordlund 2002), or whether they are created via ejection of low-mass embryos from the main reservoirs of gas in a molecular cloud (Reipurth & Clarke 2001; Bate et al. 2002). These two possibilities can be investigated by comparing the characteristics of newborn substellar objects to those of their T Tauri counterparts at stellar masses.

The paradigm for low-mass star formation begins with the collapse of a molecular cloud core onto a protostar and circumstellar accretion disk (Adams et al. 1987). The protostar continues to grow via magnetospheric accretion, whereby the inner regions of the circumstellar disk are disrupted by the stellar magnetosphere, which then channels viscously accreting material out of the disk plane and towards the star along magnetic field lines (Königl 1991; Shu et al. 1994). Signposts of this process, which have been directly observed in classical T Tauri stars (hereafter, CTTSs), include: infrared (IR) emission from dust at a range of temperatures in the disk heated by stellar irradiation and viscous dissipation (e.g., Meyer et al. (1997); Muzerolle et al. (2003a)); blue/UV continuum excess emission from the accretion shock formed as accreting material falls onto the stellar surface (Hartigan et al. 1995; Valenti et al. 1993; Gullbring et al. 1998; Calvet et al. 1998); broad permitted emission lines produced in the ballistic magnetospheric gas flows (Muzerolle et al. (2001), hereafter MCH); forbidden emission lines produced in accretion-powered winds and jets (Hartigan et al. 1995).

Recent studies have begun to examine these various signposts near and below the hydrogen burning limit to ascertain whether the same formation mechanism applies at both stellar and substellar masses. High-resolution optical spectroscopy of young brown dwarfs has indeed provided considerable evidence for magnetically-mediated disk accretion, including broad permitted emission line profiles (especially $H\alpha$) and optical continuum veiling (White & Basri (2003), hereafter, WB03; Muzerolle et al. (2003b), hereafter, M03; Jayawardhana et al. (2003b)). Furthermore, detection of IR excess emission in many objects confirms the presence of irradiated circumstellar disks (Comerón et al. 1998, 2000; Luhman 1999; Muench et al. 2001; Natta et al. 2002; Jayawardhana et al. 2003a).

In this paper, we present high-resolution spectroscopy of $H\alpha$ emission line profiles for young low-mass objects, identify likely accretion candidates, and estimate mass accretion rates through profile modeling. This work extends measurements of accretion to the lowest masses yet examined, approaching the planetary mass regime ($M/M_{\odot} \sim 0.015$), and significantly increases the number of substellar objects with accretion measurements. When these results are combined with our previous studies of accretion at higher masses, we are

able to trace the change in accretion rates from stars to brown dwarfs across two orders of magnitude in mass.

2. Observations

For this study, we considered spectroscopically confirmed low-mass members of the nearest star forming regions that are optically accessible ($I \lesssim 20$). Preference was given to objects with strong $H\alpha$ emission. The resulting sample consists of 39 members of the Taurus and Chamaeleon I star-forming regions taken from Briceño et al. (2002), Luhman et al. (2003a), Luhman (2004a,b,c), and Luhman (in preparation), which are listed in Table 1. The youth and membership of all of the objects in Taurus and Chamaeleon I have been established in these previous studies using low-resolution spectroscopy, determining spectral types from various atomic and molecular features and selecting against main sequence dwarfs or giants using gravity-sensitive K I and Na I absorption lines that are indicative of pre-main-sequence sources. The membership of some of these objects has been independently confirmed by the presence of reddening in their spectra and their positions above the main sequence for the distance of each region, which indicate that they cannot be field dwarfs in the foreground or the background of the cloud, respectively. The detections of accretion presented in this work represent additional evidence of youth, since such strong broad $H\alpha$ emission is not seen in field dwarfs.

Our targets are placed on the Hertzsprung-Russell (H-R) diagram in Figure 1 using temperatures and luminosities estimated in the studies cited above. According to the evolutionary models of Baraffe et al. (1998) and Chabrier et al. (2000), ~ 25 of these sources are brown dwarfs, one of which has a mass of only $\sim 0.01 M_{\odot}$. On the nights of 2003 December 30 through 2004 January 2, we obtained spectra of these targets with the Magellan Inamori Kyocera Echelle (MIKE) on the Magellan II 6.5 m telescope at Las Campanas Observatory. The instrument provided full coverage from 3200 to 10000 Å at a resolution near 20,000 with a 1" slit. The exposure times ranged from 300 to 3600 s.

The MIKE data were bias-subtracted and trimmed using standard IRAF¹ routines. The processed frames were then cleaned of cosmic rays with the *crutils* package. Since there was no signal in the blue camera spectra and the first few orders of the red camera spectra, we only extracted one dimensional spectra for the 22 reddest orders, providing an effective

¹IRAF is distributed by the National Optical Astronomy Observatories, which are operated by the Association of Universities for Research in Astronomy, Inc., under cooperative agreement with the National Science Foundation.

wavelength coverage of about 5700 to 10000 Å. The spectra were extracted with the *apall* routine in the IRAF *echelle* package, and wavelength calibrated using ThAr lamp spectra.

3. Analysis

3.1. Observed H α Profiles

The observed H α profiles for our entire sample are shown in Figure 2. Profile shapes and strengths closely resemble those from previous observations of young low-mass objects. Emission is detected in all of the targets; $\sim 60\%$ of them exhibit narrow ($\text{FWHM} \lesssim 200 \text{ km s}^{-1}$), symmetric profiles, while the remainder display broader, asymmetric profiles, occasionally with superimposed blueshifted or central absorption reversals. The former type of emission is likely due to chromospheric activity on the substellar surface, while the latter is probably produced in accretion flows channeled from a circumstellar disk by the substellar magnetic field (Muzerolle et al. (2000); M03; WB03). At least three objects, 2M J04554757+3028077, 2M J04141188+2811535, and 2M J11013205-7718249, show blueshifted absorption components superimposed on the accretion emission profiles, indicating accretion-powered mass loss analogous to that seen in higher-mass T Tauri stars. One of these, 2M J11013205-7718249, shows an extreme P Cygni profile, with no evident emission at blue velocities $\lesssim -50 \text{ km s}^{-1}$, and may be entirely formed in the wind. Such wind-dominated profiles are occasionally seen in higher-mass CTTSs with large mass loss rates, such as DR Tau (e.g., MCH). Since mass loss typically scales with accretion (Hartigan et al. 1995), it is somewhat surprising to see this behavior in substellar objects, given their generally small accretion rates. Substellar objects of this type are thus worthy of further scrutiny.

Based on a comparison between H α emission line equivalent widths (W_λ), H α full-widths at 10% of the peak intensity (V_{10}), and spectral types, WB03 determined an empirical boundary between accretion and chromospheric activity of $W_\lambda > 40 \text{ \AA}$ and $V_{10} > 270 \text{ km s}^{-1}$ for young low-mass objects with spectral types later than M6. In Figure 3, we examine the same issue for our sample, including for the first time objects at $M/M_\odot \lesssim 0.05$. We see a significant number of objects later than M6 with $W_\lambda > 40 \text{ \AA}$, but with V_{10} below the nominal 270 km s^{-1} threshold adopted by WB03. This has also been noted by Jayawardhana et al. (2003b), who adopted a lower limit of $V_{10} > 200 \text{ km s}^{-1}$ based on observations of three accretors with spectral types later than M6. The lower line widths are likely a reflection of intrinsically smaller accretion flow velocity fields due to the smaller object masses and radii; the maximum velocity from infall is $V_{infall} = \sqrt{2GM_*/R_*}$, which yields an upper limit to infall line widths of about 195 km s^{-1} for the lowest-mass objects in our sample. In order to define the accretor subsample, we have adopted a 10% width criterion $V_{10} > 180 \text{ km s}^{-1}$,

which is at the upper end of the most obvious break between $H\alpha$ emission characteristics. A total of 17 objects meet this criterion.

We may be missing some objects with broad accretion components that are undetectable given the signal-to-noise of our data. Using the accretion models described below, we predict a minimum measurable mass accretion rate of $\sim 10^{-12} M_{\odot} \text{yr}^{-1}$ for objects with $M \sim 0.05 M_{\odot}$ (this limit will vary somewhat with the mass of the central object because of the change in the underlying photospheric continuum). Thus, some of the objects not identified as accretors in this work may in fact still be accreting, but below this extremely low rate. However, given the significant separation of two populations apparent in the 10% width distribution, as opposed to a continuous distribution, we believe the number of missing accretors is likely to be small.

3.2. Model $H\alpha$ Profiles

Our goal in this paper is to determine mass accretion rates for our substellar sample. There are only two primary indicators currently available for this purpose: measuring veiling continuum excess or modeling $H\alpha$ emission profiles. For objects near or below the substellar limit, the former method has been applied in just a few cases by WB03 and M03. Unfortunately, veiling is unmeasurable for the large majority of very low mass objects, given their generally tiny accretion rates (M03). Thus, modeling of $H\alpha$ is the most widely applicable primary diagnostic, and we use this method here.

Previously, we have developed radiative transfer models of permitted emission line profiles for both solar-type CTTSs (MCH) and their low-mass stellar and substellar counterparts (M03). These models treat line emission produced by magnetospheric accretion flows, where gas accreting through a circumstellar disk is channeled onto the star by the stellar magnetic field. The model assumes an ideal dipolar field geometry, and a specified gas temperature distribution and mass accretion rate; the gas density distribution is determined directly from the geometry and the gas velocity as a function of the mass and radius of the star. We defer most of the theoretical details to MCH and M03.

In brief, for this paper we have adopted the same accretion model, using several values of the stellar mass (0.025 - 0.15 M_{\odot}) and radius (0.25 - 1 R_{\odot}) that are representative of our sample (see Table 1). The actual mass range will change somewhat depending on which evolutionary tracks are used; however, this should not affect our modeling applications since the model gas velocities, and, hence the line widths, are only sensitive to \sqrt{M} , and the derived masses are unlikely to be off by more than a factor of two. We employ the same

temperature constraints as those found to reproduce various emission profiles and line ratios for CTTSs with well-determined accretion rates from other observations. As we discussed in M03, this assumption should be adequate since the gas is probably heated mechanically through processes independent of spectral type. The temperature constraints result in an inverse proportionality between the gas temperature and density. Due to the lack of opacity broadening in any of the observed $H\alpha$ profiles, we can rule out $\dot{M} \gtrsim 10^{-9} M_{\odot} \text{yr}^{-1}$ (M03). For lower values of \dot{M} , the gas temperature can be fairly well-constrained; for $T \gtrsim 10,000$ K, the gas is already completely ionized, so the line flux will not change appreciably, while below this level, there is not enough line optical depth to produce emission at observed levels. Further details on the parameter constraints are found in M03; here, we apply the same methodology.

We consider the likely accretors identified in the previous section that have spectral types M6 and later. The wind-dominated object 2M J11013205-7718249 lacks emission in the blue wing, thus we cannot reliably match an accretion model and do not include it in the following analysis. For each of the remaining accretor $H\alpha$ profiles, we constructed a model by adopting the magnetospheric temperature and size constraints discussed in M03, using the model substellar mass and radius closest to the empirically determined values, and finally varying only the mass accretion rate and inclination angle to find the best match to the observed profile shape and flux. A range of accretion rates was explored, $10^{-12} < \dot{M} < 10^{-10} M_{\odot} \text{yr}^{-1}$. The lower limit corresponds to the level where accretion emission is produced at an undetectable level, while values above the upper limit would produce too much flux both in the wings (from opacity broadening) and in the line overall compared to the data in our sample. The inclination angle was varied from pole-on to edge-on orientations of the star/disk system. The comparisons were made by eye; in the cases where the profile exhibited central or blueshifted absorption components, only the high-velocity line wings unaffected by absorption were considered.

Our best model matches are shown in Figure 4, with parameters listed in Table 2. The accretion rates for these objects and the limits for the remainder of our sample are also provided in Table 1. We do not include the results for KPNO 4 as the best model match does not agree particularly well in terms of profile shape – the observed profile is quite symmetric, with a central absorption reversal strongly suggestive of chromospheric emission. The V_{10} width and EW for this object are marginal for accretion, and could also be explained by chromospheric emission broadened by rapid rotation; unfortunately, our spectrum does not have enough S/N to measure $v \sin i$.

As mentioned in M03, there is a systematic uncertainty in our model-derived \dot{M} values of about a factor of 3-5. This is mainly due to uncertainties in the size of the accretion flow,

which is not well-constrained for our particular sample. However, observations of infrared excesses around brown dwarfs in general infer inner disk hole sizes of roughly $2 - 5 R_*$, similar to our adopted value (Natta et al. 2002; Liu et al. 2003; Mohanty et al. 2004).

4. Discussion

Our results more than triple the number of known substellar accretors (those with spectral types later than M6) to 16, and extend measurements of mass accretion rates down to the lowest masses yet identified. The new accretion rates for our sample of low-mass stars and brown dwarfs, combined with previous estimates for other brown dwarfs and more massive stars, are plotted as a function of mass in Figure 5. The accretion rates for substellar objects are extremely small, mostly $< 10^{-10} M_\odot \text{yr}^{-1}$, several of which are among the lowest values measured to date at $\dot{M} = 4 - 5 \times 10^{-12} M_\odot \text{yr}^{-1}$. These data continue a trend that we have noted previously for the more massive objects in which mass accretion rates depend steeply on mass; here, we find a correlation of $\dot{M} \propto M^{2.1}$. In addition, the change in accretion rate with mass is fairly continuous across six orders of magnitude in \dot{M} and more than two orders of magnitude in mass, which suggests that the same formation mechanism is responsible for both the low- and high-mass objects. Folding in previous work mentioned above, and our own studies of intermediate mass young stars (Calvet et al. 2004), there is now significant evidence that the disk accretion paradigm applies to a range of over two orders of magnitude in mass, from $0.02 - 3 M_\odot$. Thus, free-floating stellar and substellar objects in this mass range, comprising all but the most massive O and B stars, likely form from the collapse of a molecular cloud core onto an accretion disk and central object.

There is considerable scatter in \dot{M} for a given mass all across the mass spectrum, as has been noted previously for the higher-mass objects. Most of this scatter probably reflects intrinsic differences from source to source, and may be due to age differences, since viscous evolution expects a general decrease in the accretion rate with time (Hartmann et al. 1998), or differences in initial conditions. We note that the accretion rate measurements for low mass members of Ophiuchus from Natta et al. (2004) appear to be larger on average by about a factor of 5-10 than those in Taurus, Chamaeleon I, and IC 348. This may be an indication of the slightly younger age of Ophiuchus, or possibly different initial conditions such as the larger envelope infall rates that characterize protostellar objects in that region.

Our results also imply that objects down to masses of $0.02 M_\odot$ harbor significant, ordered magnetic fields. Accretion infall cannot occur unless there is a magnetic field of sufficient strength to truncate the inner disk and channel material onto the surface of the substellar object. Given the model-derived mass accretion rates, inner disk hole size implied

by our adopted inner magnetospheric radius, and empirical mass and radius estimates, we predict magnetic field strengths on the order of 100-200 G for the lowest-mass accretors in our sample, using the theoretical relations given by Königl (1991). Significant magnetic fields are also likely to exist on the nonaccretors, given their signatures of chromospheric activity similar to that seen in M and L field dwarfs (e.g. Mohanty & Basri 2003).

Finally, given the object masses and typical ages of ~ 1 Myr, the mass accretion rates in Figure 5 will have little or no effect on the remaining history of the young stars and brown dwarfs we have considered. Presumably, most of the mass is accreted in the earliest phases of evolution, either in the initial collapse of the cloud core or via outbursts initiated by disk instabilities. As such, it will be important to eventually identify and study embedded protostellar counterparts at the lowest masses.

We thank the staff at Las Campanas Observatory for their support of these observations. K. L. was supported by grant NAG5-11627 from the NASA Long-Term Space Astrophysics program. 2MASS is a joint project of the University of Massachusetts and the Infrared Processing and Analysis Center/California Institute of Technology, funded by the National Aeronautics and Space Administration and the National Science Foundation.

REFERENCES

- Adams, F. C., Lada C. J., & Shu, F. H. 1987, *ApJ*, 312, 788
- Baraffe, I., Chabrier, G., Allard, F., & Hauschildt, P. H. 1998, *A&A*, 337, 403
- Bate, M. R., Bonnell, I. A., & Bromm, V. 2002, *MNRAS*, 332, L65
- Briceño, C., Luhman, K. L., Hartmann, L., Stauffer, J. R., & Kirkpatrick, J. D. 2002, *ApJ*, 580, 317
- Calvet, N. & Gullbring, E. 1998, *ApJ*, 509, 802 (CG98)
- Calvet, N., Muzerolle, J., Briceño, C., Fernández, J., Hartmann, L., Saucedo, J. L., & Gordon, K. D. 2004, *ApJ*, in press
- Chabrier, G., Baraffe, I. Allard, F., & Hauschildt, P. H. 2000, *ApJ*, 542, 464
- Comerón, F., Neuhäuser, R., & Kaas, A. A. 2000, *A&A*, 359, 269
- Comerón, F., Rieke, G. H., Claes, P., Torra, J., & Laureijs, R. J. 1998, *A&A*, 335, 522

- Gullbring, E., Hartmann, L., Briceño, C., & Calvet, N. 1998, *ApJ*, 492, 323
- Hartigan, P., Edwards, S., & Ghandour, L. 1995, *ApJ*, 452, 736
- Hartmann, L., Calvet, N., Gullbring, E., & D'Alessio, P. 1998, *ApJ*, 495, 385
- Jayawardhana, R., Ardila, D. R., Stelzer, B., & Haisch, K. E. 2003a, *AJ*, 126, 1515
- Jayawardhana, R., Mohanty, S., & Basri, G. 2003b, *ApJ*, 592, 282
- Königl, A. 1991, *ApJ*, 370, L39
- Liu, M. C., Najita, J., & Tokunaga, A. T. 2003, *ApJ*, 585, 372
- Luhman, K. L. 1999, *ApJ*, 525, 466
- Luhman, K. L. 2004a, *ApJ*, 602, 816
- Luhman, K. L. 2004b, *ApJ*, in press
- Luhman, K. L. 2004c, *ApJ*, in press
- Luhman, K. L., Briceño, C., Stauffer, J. R., Hartmann, L., Barrado y Navascués, D., & Nelson, C. 2003a, *ApJ*, 590, 348
- Luhman, K. L., Stauffer, J. R., Muench, A. A., Rieke, G. H., Lada, E. A., Bouvier, J., & Lada, C. J. 2003b, *ApJ*, 593, 1093
- Meyer, M. R., Calvet, N., & Hillenbrand, L. A. 1997, *AJ*, 114, 288
- Mohanty, S., Jayawardhana, R., Natta, A., Fujiyoshi, T., Tamura, M., & Barrado y Navascués, D. 2004, *ApJ*, in press
- Mohanty, S. & Basri, G. 2003, *ApJ*, 583, 451
- Muench, A. A., Alves, J., Lada, C. J., & Lada, E. A. 2001, *ApJ*, 558, L51
- Muzerolle, J., Briceño, C., Calvet, N., Hartmann, L., Hillenbrand, L. A., & Gullbring, E. 2000, *ApJ*, 545, L141
- Muzerolle, J., Calvet, N., & Hartmann, L. 1998a, *ApJ*, 492, 743
- Muzerolle, J., Calvet, N., & Hartmann, L. 2001, *ApJ*, 550, 944 (MCH)
- Muzerolle, J., Calvet, N., Hartmann, L., & D'Alessio, P. 2003a, *ApJ*, 597, L149

- Muzerolle, J., Hartmann, L., & Calvet, N. 1998b, *AJ*, 116, 455
- Muzerolle, J., Hillenbrand, L., Calvet, N., Briceño, C., & Hartmann, L. 2003b, *ApJ*, 592, 266 (M03)
- Natta, A., Testi, L., Comerón, F., Oliva, E., D'Antona, F., Baffa, C., Comoretto, G., & Gennari, S. 2002, *A&A*, 393, 597
- Natta, A., Testi, L., Muzerolle, J., Randich, S., Comerón, F., & Persi, P. 2004, *A&A*, 424, 603
- Padoan, P., & Nordlund, Å. 2002, *ApJ*, 576, 870
- Reipurth, B. & Clarke, C. 2001, *AJ*, 122, 432
- Shu, F., Najita, J., Ostriker, E., Wilkin, F., Ruden, S., & Lizano, S. 1994, *ApJ*, 429, 781
- Valenti, J. A., Basri, G., & Johns, C. M. 1993, *AJ*, 106, 2024
- White, R. J. & Basri, G. 2003, *ApJ*, 582, 1109 (WB03)
- White, R. J. & Ghez, A. M. 2001, *ApJ*, 556, 265

Table 1. Data for Observed Sample

ID	α (J2000) ^a	δ (J2000) ^a	Spectral Type ^b	$T_{\text{eff}}^{\text{b}}$ (K)	$L_{\text{bol}}^{\text{b}}$ (L_{\odot})	Radius (R_{\odot})	Mass (M_{\odot})	$W_{\lambda}(\text{H}\alpha)$ (\AA)	H α 10% Width (km s^{-1})	log \dot{M} ($M_{\odot} \text{ yr}^{-1}$)
KPNO 4	04 27 28.00	+26 12 05.3	M9.5	2300	0.0023	0.30	0.011	-38.4	192	<-12
KPNO 12	04 19 01.27	+28 02 48.7	M9	2400	0.00082	0.17	0.020	-66.8	206	-11.4
KPNO 6	04 30 07.24	+26 08 20.8	M8.5	2555	0.0021	0.23	0.025	-41.1	235	-11.4
KPNO 7	04 30 57.19	+25 56 39.5	M8.25	2632	0.0033	0.28	0.030	-31.1	220	-11.4
2M J11013205-7718249	11 01 32.05	-77 18 25.0	M8	2710	0.0044	0.30	0.035	-66.8	283	...
CHSM 17173	11 17 23.83	-76 24 08.6	M8	2710	0.011	0.48	0.030	-85.3	132	<-12
2M J04414825+2534304	04 41 48.25	+25 34 30.5	M7.75	2752	0.0086	0.41	0.035	-233.7	256	-11.3
Cha H α 1	11 07 16.69	-77 35 53.3	M7.75	2752	0.013	0.50	0.035	-118.3	192	-11.3
Cha H α 7	11 07 37.76	-77 35 30.8	M7.75	2752	0.012	0.48	0.035	-26.0	114	<-12
CFHT 3	04 36 38.94	+22 58 11.9	M7.75	2752	0.0088	0.41	0.035	-10.5	110	<-12
KPNO 2	04 18 51.16	+28 14 33.2	M7.5	2795	0.0057	0.32	0.045	-3.9	87	<-12
KPNO 5	04 29 45.68	+26 30 46.8	M7.5	2795	0.019	0.59	0.040	-26.4	133	<-12
2M J04390396+2544264	04 39 03.96	+25 44 26.4	M7.25	2838	0.019	0.57	0.050	-102.0	215	-11.3
2M J04381486+2611399	04 38 14.86	+26 11 39.9	M7.25	2838	0.0018	0.18	0.070	-47.0	200	-10.8
Cha H α 11	11 08 29.27	-77 39 19.8	M7.25	2838	0.0045	0.28	0.055	-14.3	224	-11
2M J11011926-7732383	11 01 19.27	-77 32 38.3	M7.25	2838	0.020	0.59	0.050	-10.1	96	<-12
CFHT 4	04 36 38.94	+22 58 11.9	M7	2880	0.054	0.94	0.060	-129.3	274	-11.3
Cha H α 12	11 06 38.00	-77 43 09.1	M6.5	2935	0.028	0.65	0.075	-14.6	133	<-12
ISO 138	11 08 18.51	-77 30 40.8	M6.5	2935	0.0081	0.35	0.065	-12.4	120	<-12
ISO 217	11 09 52.16	-76 39 12.8	M6.25	2962	0.028	0.64	0.080	-66.1	334	-10
Cha H α 10	11 08 24.04	-77 39 30.0	M6.25	2962	0.0089	0.36	0.070	-7.1	91	<-12
2M J04141188+2811535	04 14 11.88	+28 11 53.5	M6.25	2962	0.019	0.53	0.075	-250.0	362	-10
CHSM 7869	11 06 32.77	-76 25 21.1	M6	2990	0.028	0.39	0.070	-72.0	300	-10
KPNO 14	04 33 07.81	+26 16 06.6	M6	2990	0.11	1.2	0.10	-14.0	140	<-12
KPNO 3	04 26 29.39	+26 24 13.8	M6	2990	0.020	0.53	0.080	-144.6	290	-10
ISO 252	11 10 41.42	-77 20 48.1	M6	2990	0.027	0.62	0.080	-173.1	274	-10
2M J11070324-7610565	11 07 03.24	-76 10 56.6	M6	2990	0.013	0.43	0.070	-9.3	169	<-12
2M J11080234-7640343	11 08 02.35	-76 40 34.4	M6	2990	0.024	0.58	0.080	-5.0	120	<-12
2M J11075993-7715317	11 07 59.93	-77 15 31.8	M5.75	3024	0.067	0.95	0.12	-8.4	178	<-12
2M J11072443-7743489	11 07 24.44	-77 43 49.0	M5.75	3024	0.042	0.75	0.11	-8.8	114	<-12
2M J11173792-7646193	11 17 37.93	-76 46 19.4	M5.75	3024	0.013	0.42	0.080	-11.8	125	<-12
2M J04554801+3028050	04 55 48.01	+30 28 05.0	M5.6	3014	0.014	0.44	0.075	-14.0	150	<-12
2M J10561638-7630530	10 56 16.38	-76 30 53.0	M5.6	3014	0.031	0.64	0.10	-41.4	283	-10.8
2M J10580597-7711501	10 58 05.98	-77 11 50.1	M5.25	3091	0.018	0.47	0.10	-5.0	137	<-12
2M J04554757+3028077	04 55 47.57	+30 28 07.7	M4.75	3161	0.098	1.0	0.20	-24.5	320	...
T23	11 06 59.07	-77 18 53.6	M4.25	3138	0.12	1.2	0.18	-7.0	247	...
T3W	10 55 59.73	-77 24 39.9	M3.5	3850	0.27	1.2	0.73	-9.5	259	...
CHXR49 NE	11 11 54.00	-76 19 31.1	M2.5	3430	0.34	1.7	0.44	0	0	...
T3E	10 55 59.73	-77 24 39.9	M0.5	3342	0.35	-8.9	247	...

Note. — Units of right ascension are hours, minutes, and seconds, and units of declination are degrees, arcminutes, and arcseconds.

^a2MASS Point Source Catalog.

^bBriceño et al. (2002), Luhman et al. (2003a), Luhman (2004a), Luhman (2004b), Luhman (2004c), and Luhman (in preparation).

Table 2. H α Model Parameters for Accretor Subsample

ID	M_* (M_\odot)	R_* (R_\odot)	T_{eff} (K)	i ($^\circ$)	$\log \dot{M}$ ($M_\odot \text{ yr}^{-1}$)
KPNO 12	0.025	0.25	2600	45	-11.4
KPNO 6	0.025	0.25	2600	60	-11.4
KPNO 7	0.025	0.25	2600	75	-11.4
2M J04414825+2534304	0.025	0.25	2600	60	-11.3
Cha H α 1	0.025	0.25	2600	45	-11.3
2M J04390396+2544264	0.025	0.25	2600	70	-11.3
2M J04381486+2611399	0.05	0.5	3000	60	-10.8
Cha H α 11	0.05	0.5	3000	30	-11
CFHT 4	0.025	0.25	2600	55	-11.3
ISO 217	0.05	0.5	3000	65	-10 ^a
2M J04141188+2811535	0.05	0.5	3000	55	-10
CHSM 7869	0.15	1.0	3000	85	-10
KPNO 3	0.15	1.0	3000	60	-10
ISO 252	0.15	1.0	3000	45	-10
2M J10561638-7630530	0.05	0.5	3000	60	-10.8

Note. — All models calculated with magnetospheric radii $R_{mag} = 2.2-3 R_\odot$ and maximum temperature $T_{max} = 12,000$ K.

^aCalculated with modified temperature distribution; see text.

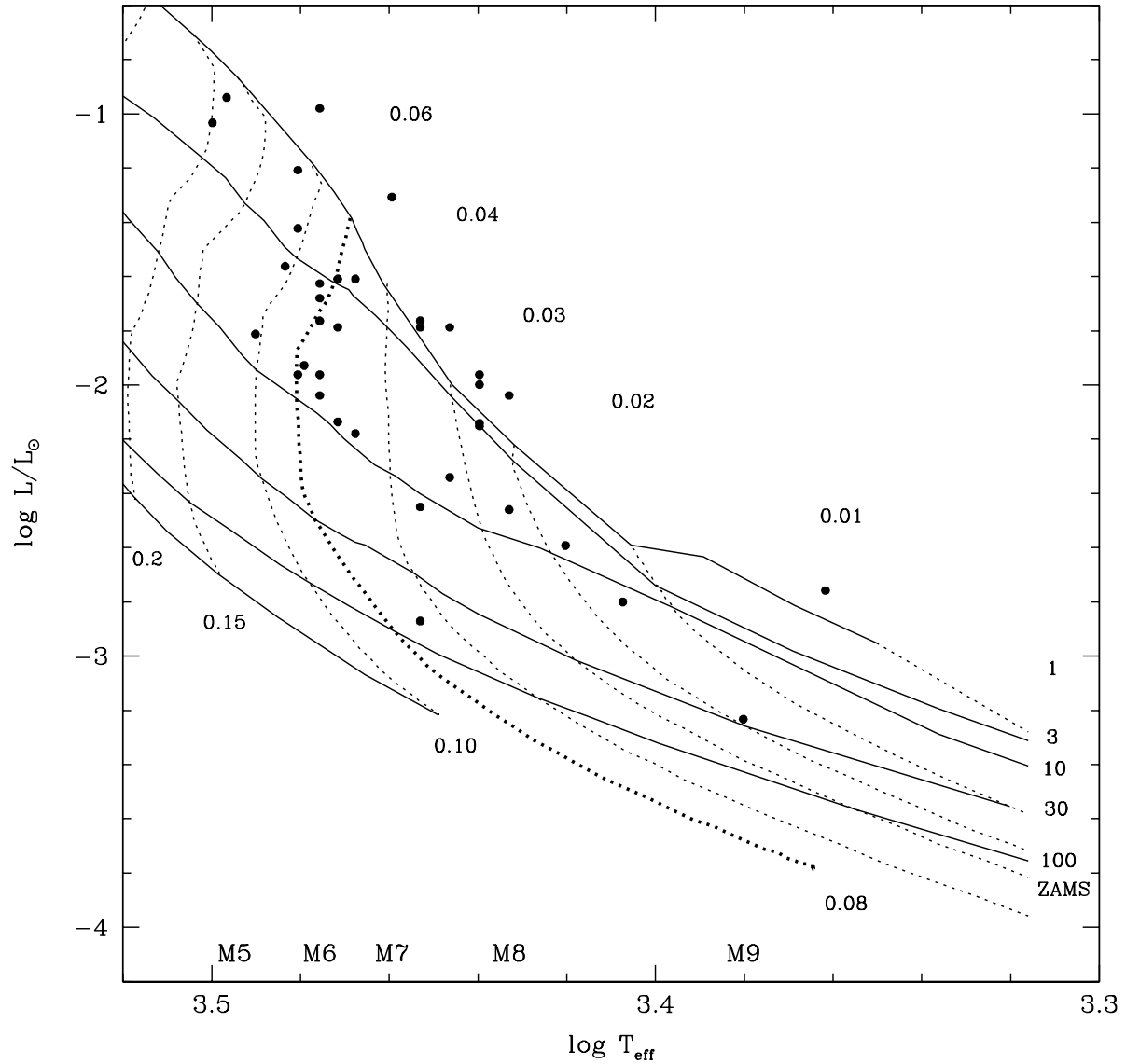


Fig. 1.— H-R diagram for the targets of the high-resolution spectroscopy in this work shown with the theoretical evolutionary models of Baraffe et al. (1998) ($M/M_{\odot} > 0.1$) and Chabrier et al. (2000) ($M/M_{\odot} \leq 0.1$), where the mass tracks (*dotted lines*) and isochrones (*solid lines*) are labeled in units of M_{\odot} and Myr, respectively.

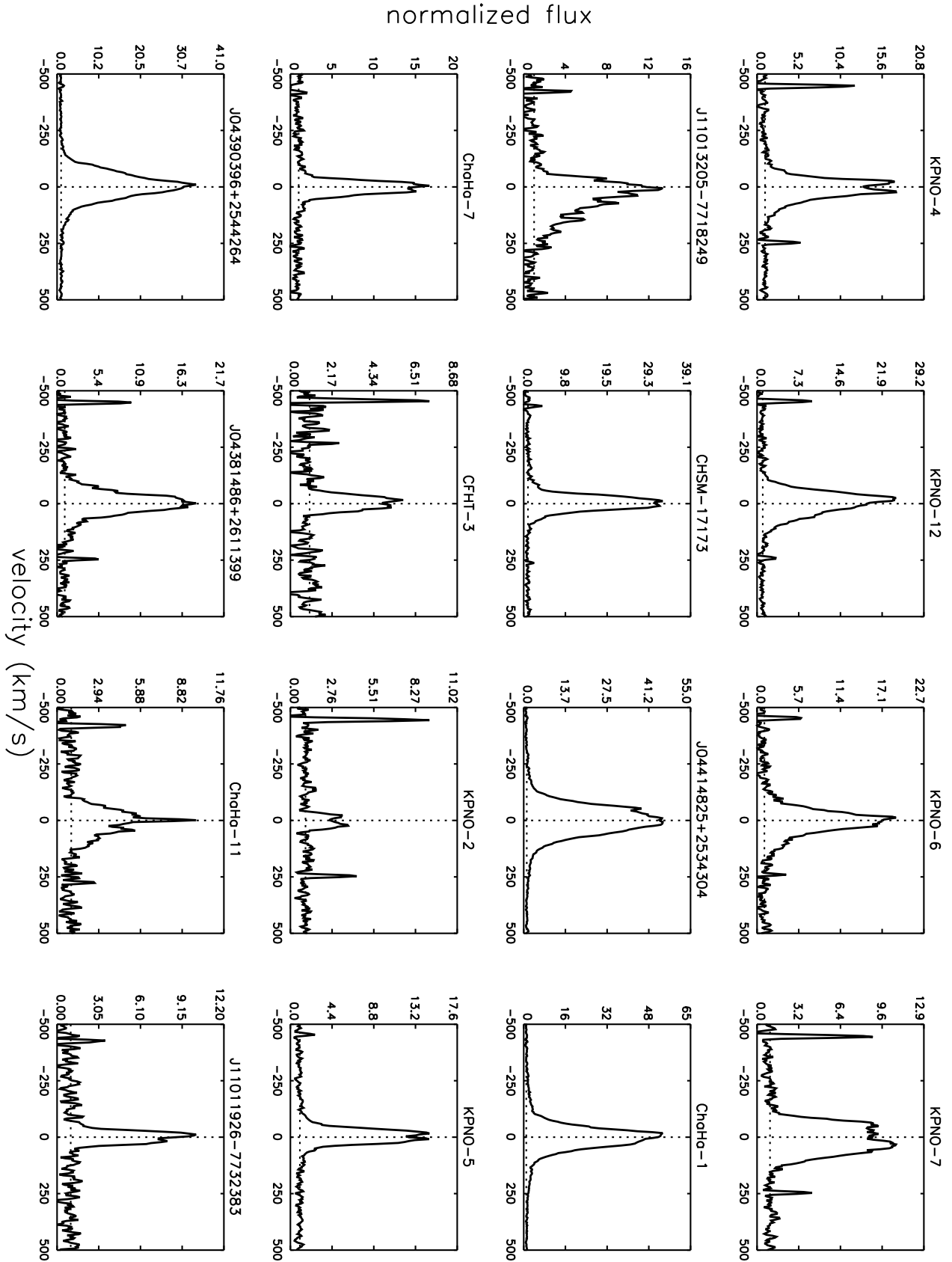


Fig. 2.— Observed H α emission line profiles. The spikes close to -500 and +250 km/s seen in some spectra (e.g. J04381486+2611399 and KPNO-2) are sky lines that could not be

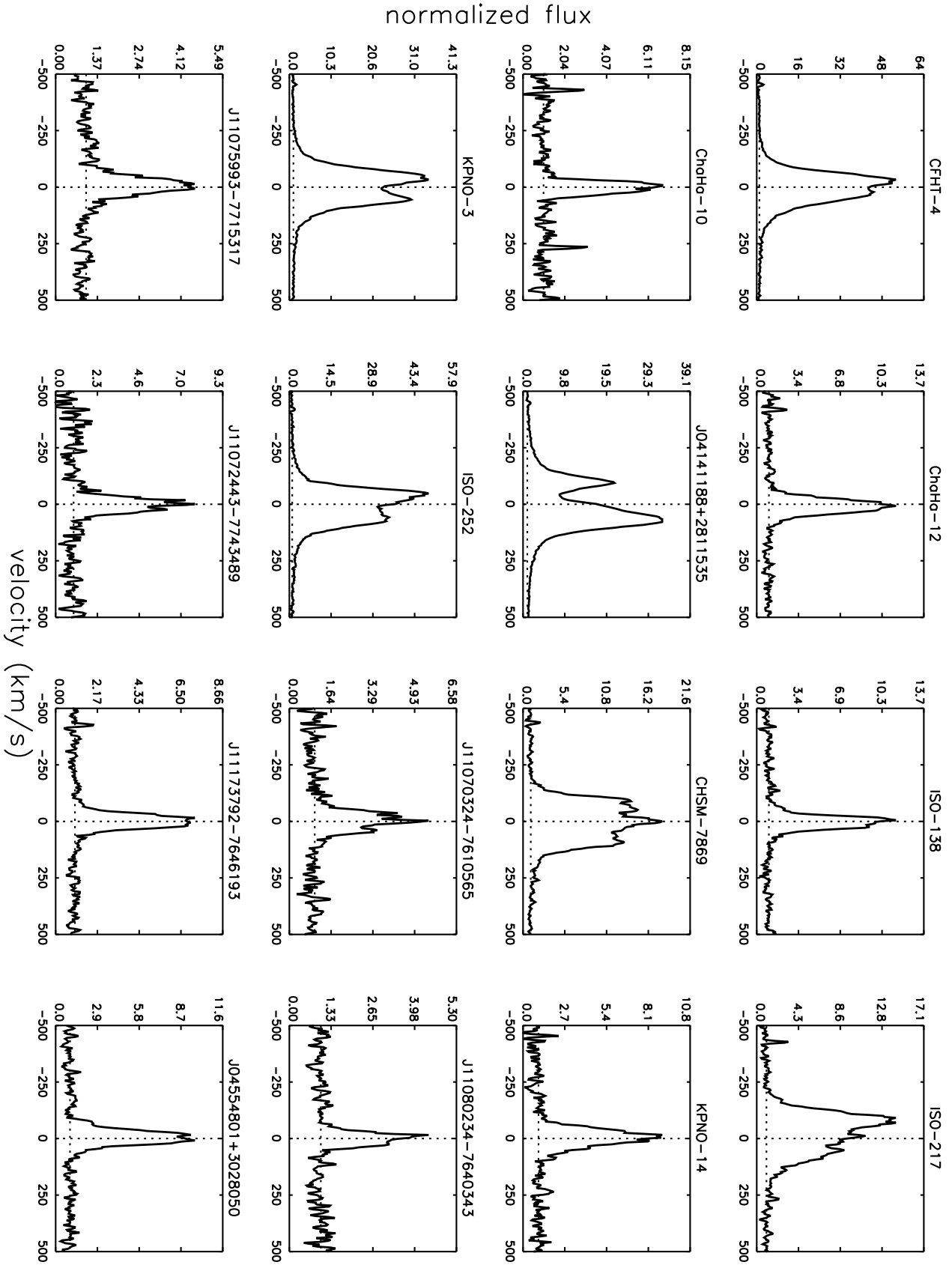


Fig. 2.— Continued.

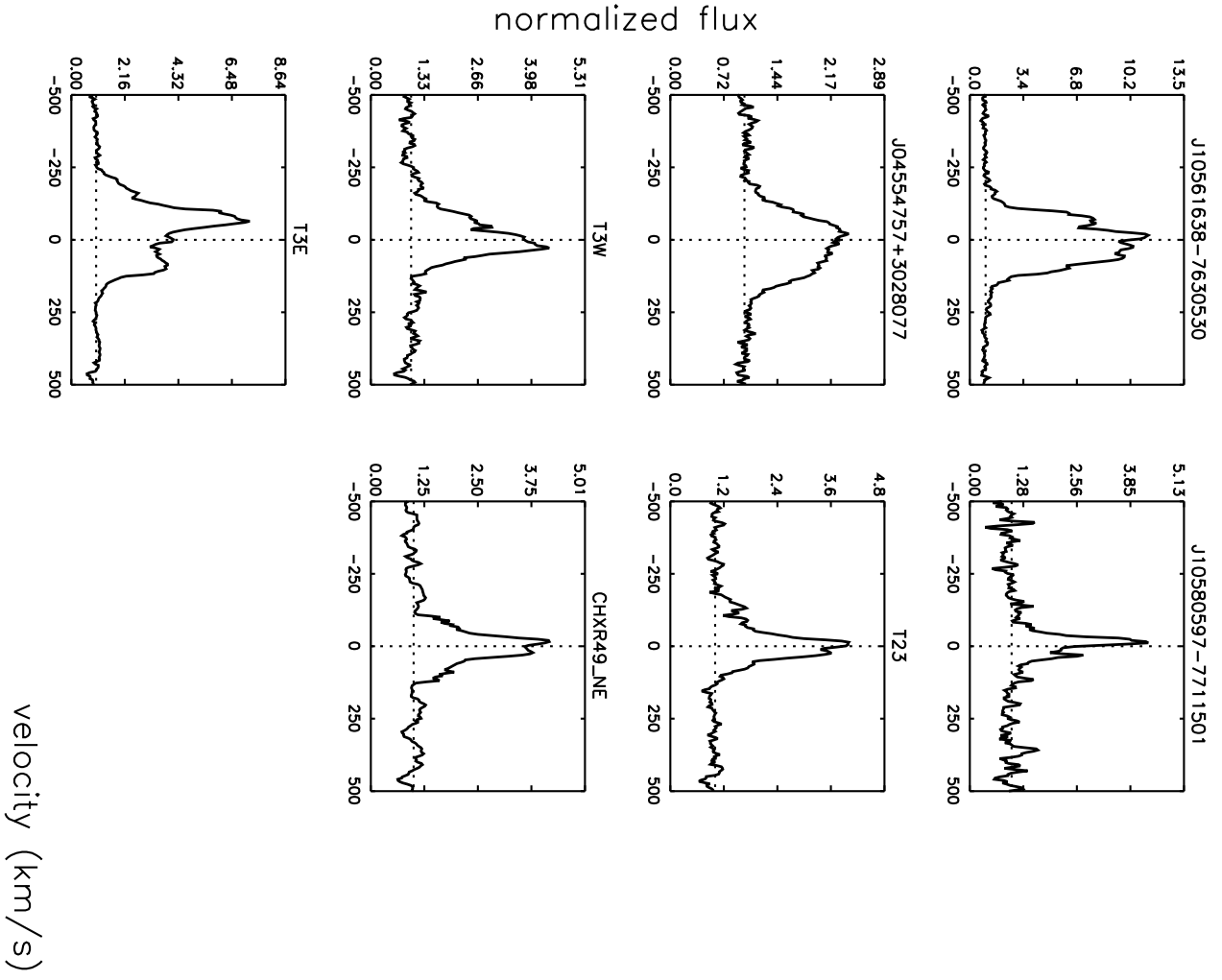


Fig. 2.— Continued.

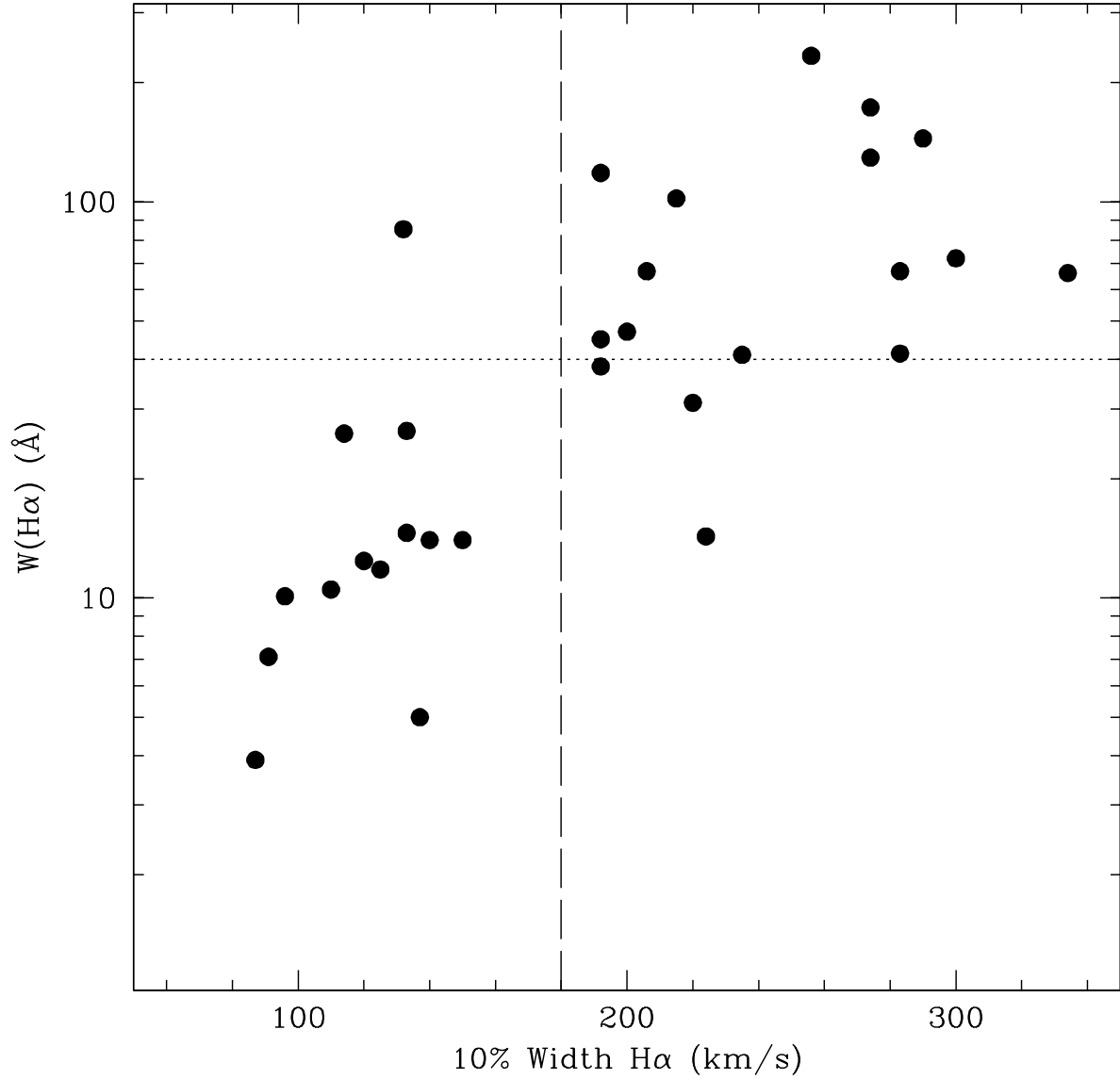


Fig. 3.— Equivalent widths of H α vs. the 10% widths of H α for our sample of young stars with spectral types M6 and later ($M/M_{\odot} \lesssim 0.08$). The horizontal dotted line indicates the $W(\text{H}\alpha) = 40\text{\AA}$ nominal limit between weak-lined T Tauri stars and Classical T Tauri stars for spectral types M6-7.5, as defined by White & Basri (2003). The vertical dashed line is our adopted threshold separating accretors and chromospherically active stars.

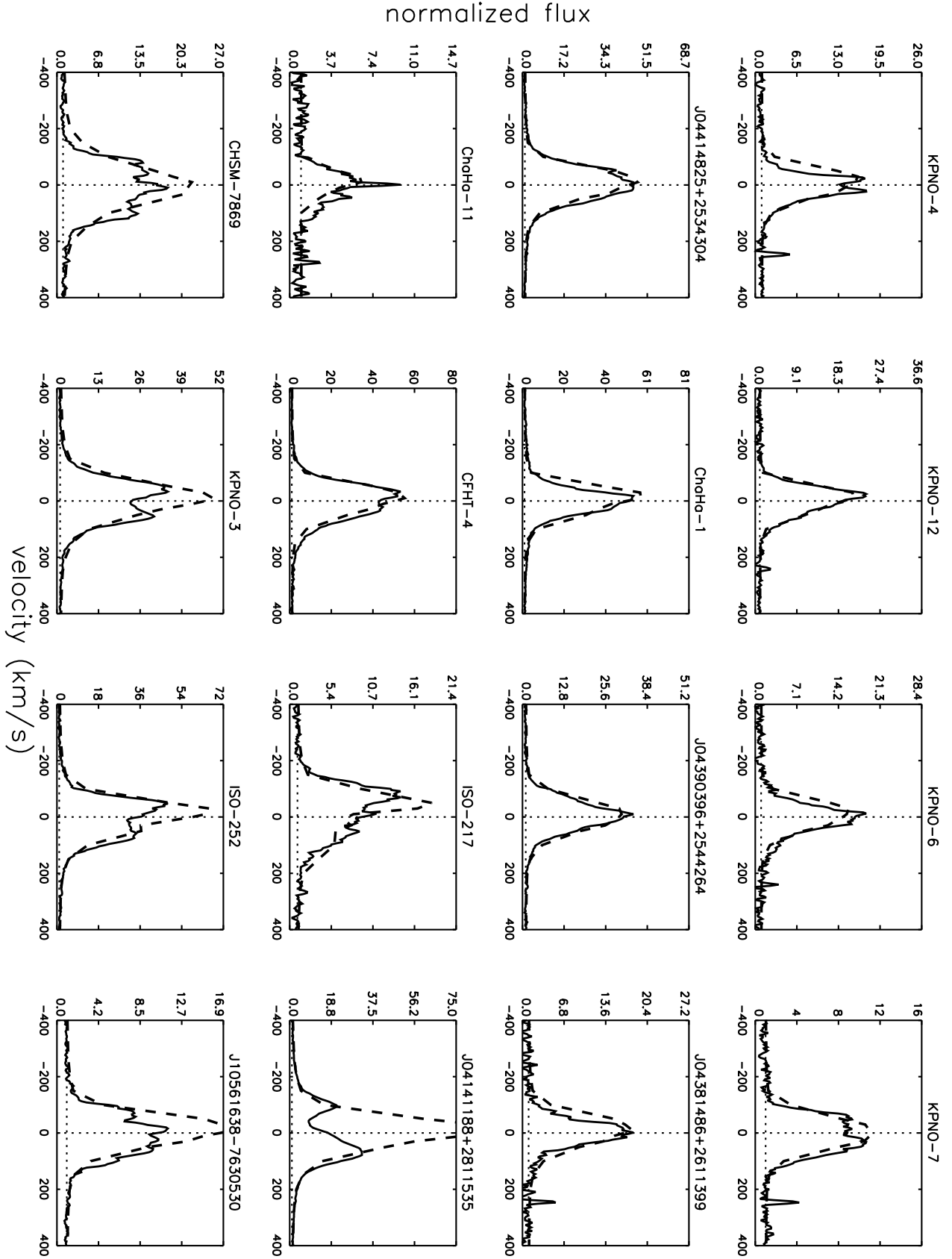


Fig. 4.— Comparisons of observed (*solid*) and model (*dashed*) H α emission line profiles for objects in our sample that have profiles indicative of accretion (Table 2).

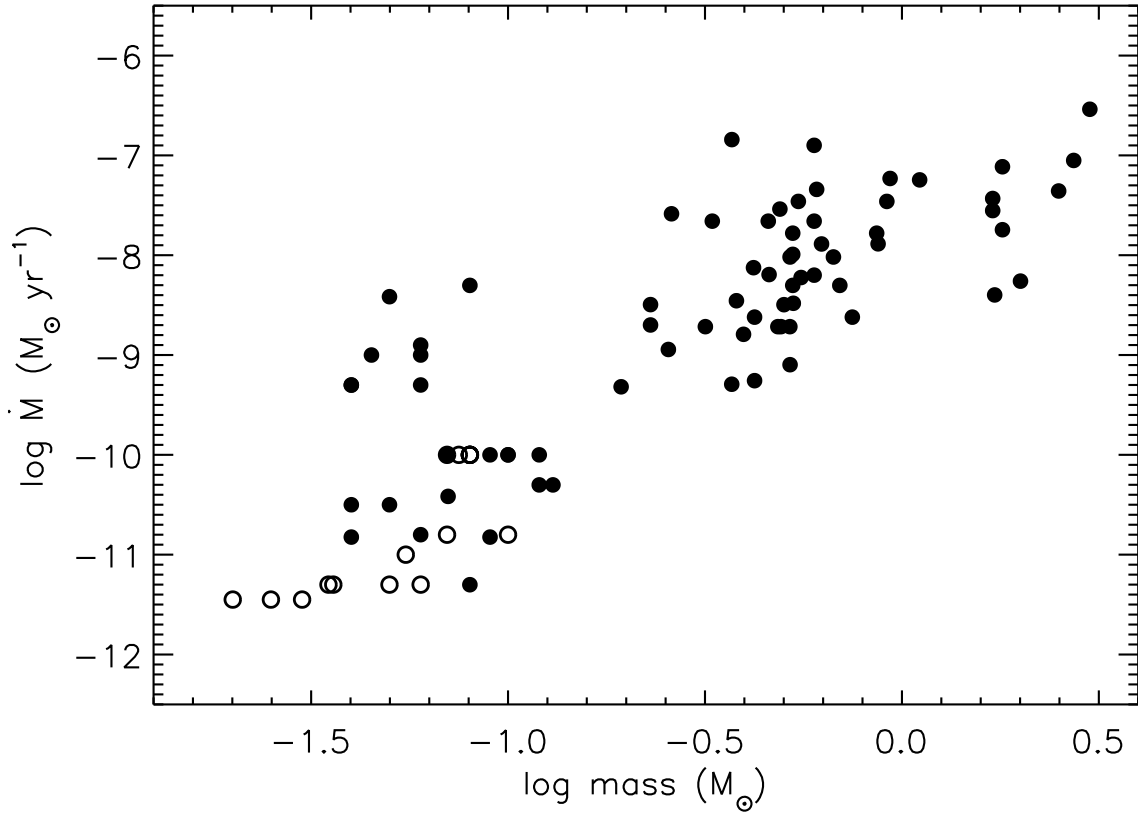


Fig. 5.— Mass accretion rate as a function of mass. Filled circles are from Gullbring et al. (1998), White & Ghez (2001), WB03, M03, Calvet et al. (2004), and Natta et al. (2004), and open circles are from this work.